

This discussion paper is/has been under review for the journal Biogeosciences (BG).
Please refer to the corresponding final paper in BG if available.

Processes determining the marine alkalinity and carbonate saturation distributions

B. R. Carter¹, J. R. Toggweiler², R. M. Key¹, and J. L. Sarmiento¹

¹Atmospheric and Oceanic Sciences Program, Princeton University, Princeton, NJ, USA

²Geophysical Fluid Dynamics Laboratory, National Oceanic and Atmospheric Administration, P.O. Box 308, Princeton, NJ, 08542, USA

Received: 1 July 2014 – Accepted: 3 July 2014 – Published: 21 July 2014

Correspondence to: B. R. Carter (br Carter@princeton.edu) and J. Sarmiento (jls@princeton.edu)

Published by Copernicus Publications on behalf of the European Geosciences Union.

Title Page

Abstract

Introduction

Conclusions

References

Tables

Figures



Back

Close

Full Screen / Esc

Printer-friendly Version

Interactive Discussion



Abstract

We introduce a composite tracer, Alk*, that has a global distribution primarily determined by CaCO₃ precipitation and dissolution. Alk* also highlights riverine alkalinity plumes that are due to dissolved calcium carbonate from land. We estimate the Arctic receives approximately twice the riverine alkalinity per unit area as the Atlantic, and 8 times that of the other oceans. Riverine inputs broadly elevate Alk* in the Arctic surface and particularly near river mouths. Strong net carbonate precipitation lowers basin mean Indian and Atlantic Alk*, while upwelling of dissolved CaCO₃ rich deep waters elevates Northern Pacific and Southern Ocean Alk*. We use the Alk* distribution to estimate the carbonate saturation variability resulting from CaCO₃ cycling and other processes. We show regional variations in surface carbonate saturation are due to temperature changes driving CO₂ fluxes and, to a lesser extent, freshwater cycling. Calcium carbonate cycling plays a tertiary role. Monitoring the Alk* distribution would allow us to isolate the impact of acidification on biological calcification and remineralization.

1 Introduction

Our goal is to use high-quality total alkalinity (A_T) observations to examine the effects of carbonate cycling on marine A_T and carbonate mineral saturation states. The marine A_T distribution is affected by the cycling of carbonate, freshwater, and organic matter, so we develop the quasi-conservative tracer Alk* to isolate the influences carbonate cycling. Alk* is estimated by adjusting A_T to remove the influences of organic matter cycling, and then subtracting a salinity-based estimate of what the adjusted A_T would be if the net influence of carbonate cycling were uniform in the ocean. We investigate the global Alk* distribution using a dataset we created by merging the PACIFICA (Suzuki et al., 2013), GLODAP, and CARINA discrete data products (Key et al., 2004,

BGD

11, 11139–11178, 2014

Processes determining marine alkalinity

B. R. Carter et al.

Title Page

Abstract

Introduction

Conclusions

References

Tables

Figures



Back

Close

Full Screen / Esc

Printer-friendly Version

Interactive Discussion



2010; Velo et al., 2009). We have combined and gridded these data products using methods detailed in Supplement document SA.

This study is motivated in part by ocean acidification. With marine carbonate saturation decreasing due to anthropogenic carbon uptake, it is important to understand the degree to which carbonate cycling impacts marine carbonate saturations and vice versa. In this paper we use Alk^* to show net carbonate precipitation and dissolution variability is not a dominant control for carbonate saturation variability. We will address the converse question in future work with Alk^* .

We derive Alk^* in Sect. 2. In Sect. 3 we discuss processes that govern the Alk^* distribution globally, by ocean basin, and regionally. In Sect. 4 we define a metric to quantify the influence of various processes over the marine calcium carbonate saturation state. We use this metric with our gridded dataset and Alk^* to determine the relative importance of the various controls in the ocean and at the ocean surface. We summarize in Sect. 5.

2 The Alk^* tracer

Dickson (1981) defines total alkalinity as the concentration excess “of proton acceptors formed from weak acids ($\text{pK} \leq 4.5$) relative to proton donors (weak bases with $\text{pK} > 4.5$)” at a reference temperature, pressure, and ionic strength. It can be thought of as a measure of how well buffered seawater is against changes in pH. This operational definition gives A_T several properties that make it an especially useful carbonate system parameter:

1. It mixes conservatively,
2. ... and is therefore diluted and concentrated linearly by evaporation and precipitation.
3. It responds in predictable ways to calcium carbonate cycling

BGD

11, 11139–11178, 2014

Processes determining marine alkalinity

B. R. Carter et al.

Title Page

Abstract

Introduction

Conclusions

References

Tables

Figures



Back

Close

Full Screen / Esc

Printer-friendly Version

Interactive Discussion



4. ... as well as organic matter formation and remineralization.

5. It is not changed by the exchange of heat or carbon dioxide.

We are primarily interested in the cycling of biogenic carbonates, item 3 in our list. It is therefore useful to define a tracer that removes the majority of the influences of organic matter (item 4) and freshwater cycling (item 2) while still mixing and responding to calcium carbonate cycling linearly.

The influence of organic matter formation on A_T is due primarily to the biologically-driven marine nitrogen cycle. We provide simplified nitrogen cycle Reactions (R1)–(R3) with proton-accepting bases that represent a positive contribution for A_T indicated with curly brackets.



Organic matter incorporates the ammonia (NH_3) produced by nitrification, making it slightly alkaline (Hernández-Ayon et al., 2007). However, organic matter is typically remineralized in-situ or exported, so it is generally assumed that the net uptake of nitrate corresponds to a 1 : 1 release of proton acceptors in these reactions (e.g. OH^-). This observation led Brewer and Goldman (1976) to propose the idea of “potential alkalinity” as the sum of A_T and nitrate with the aim of creating a tracer that responds to the cycling of calcium carbonate without changing in response to organic matter cycling. Feely et al. (2002) used a variant that relies on the empirical relationship between dissolved calcium concentrations, A_T , and nitrate determined by Kanamori and Ikegami (1982). This variant has the advantage of implicitly accounting for the A_T changes created by the exchange of numerous other components of marine organic matter besides

BGD

11, 11139–11178, 2014

**Processes
determining marine
alkalinity**

B. R. Carter et al.

Title Page

Abstract

Introduction

Conclusions

References

Tables

Figures

◀

▶

◀

▶

Back

Close

Full Screen / Esc

Printer-friendly Version

Interactive Discussion



nitrate (e.g. sulfate and phosphate). While the empirical relationship measured may be specific to the elemental ratios of the North Pacific, Wolf-Gladrow et al. (2007) provide a theoretical derivation from Redfield ratios and obtain a similar value. We also use the ratio found by Kanamori and Ikegami (1982) to define potential alkalinity (A_P).

$$A_P = A_T + 1.26 * [\text{NO}_3^-] \quad (1)$$

The sensitivity of the A_T distribution to freshwater cycling is due primarily to the dilution or concentration of the large background A_T fraction that does not participate in carbonate cycling on timescales of ocean mixing. However, freshwater sources such as ground water and river water can also be rich in dissolved carbonates and represent an oceanic A_T source that we consider with our tracer. We therefore use a salinity-normalization similar to the approach of Robbins (2001) to remove the large background fraction of surface A_T without removing A_T from dissolved carbonates in river water and groundwater. We accomplish this by subtracting our estimate of the passive conservative potential alkalinity (A_P^C), that we define as:

$$A_P^C \equiv S \frac{\overline{A_P}}{\overline{S}} \quad (2)$$

Here, terms with a bar are reference values chosen as the mean value for those properties in the top 50 m of the ocean. We obtain a volume-weighted surface $\overline{A_P}$ to \overline{S} ratio of 66.4 from our gridded dataset. The mean surface values are chosen to capture the impact of freshwater cycling where precipitation and evaporation occur. In Supplement document SB, we estimate this approach removes 97.5% of the influence of freshwater cycling on potential alkalinity and reduces the influence of freshwater cycling on Alk^* to less than 1% of the Alk^* variability.

Processes determining marine alkalinity

B. R. Carter et al.

Title Page

Abstract

Introduction

Conclusions

References

Tables

Figures

◀

▶

◀

▶

Back

Close

Full Screen / Esc

Printer-friendly Version

Interactive Discussion



In total, we define Alk^* as the deviation of potential alkalinity from A_P^C ,

$$\text{Alk}^* \equiv A_P - A_P^C \quad (3)$$

$$\equiv A_P - \frac{A_P^C}{S} S \quad (4)$$

$$\equiv A_P - 66.4 \times S \mu\text{mol kg}^{-1} \quad (5)$$

where Alk^* has alkalinity units. The Alk^* distribution is attributable primarily to carbonate cycling plus the small residual variation due to freshwater cycling that is not removed by subtracting A_P^C . Mean global surface Alk^* is zero by definition, and negative Alk^* is possible when potential alkalinity is less than expected from salinity. For reference, more than 95 % of our gridded Alk^* dataset falls between -35 and $220 \mu\text{mol kg}^{-1}$.

Alk^* mixes conservatively (demonstrated in Supplement document SC), retains the 2 : 1 change of A_T to dissolved inorganic carbon (C_T) with formation or dissolution of calcium carbonate, and preserves dissolved carbonate alkalinity entering the ocean in river water. By contrast, typical salinity normalization (e.g. sA_P , which multiplies potential alkalinity by the ratio between the in situ salinity and reference salinity) does not mix conservatively, has a variable response to carbonate production, and yields an undefined value for a riverine end-member with zero salinity and non-zero A_P . The Alk^* and sA_P distributions are broadly similar despite these differences in approach, though discrepancies between them are pronounced where there are large concentrations of riverine water. Figure 1 shows differences between individual sA_P estimates and the global mean estimate $\overline{sA_P}$ against the differences between individual Alk^* estimates and the global mean estimate $\overline{\text{Alk}^*}$. This figure reveals that the non-linearity of sA_P can bias estimates high by $> 2000 \mu\text{mol kg}^{-1}$.

BGD

11, 11139–11178, 2014

Processes determining marine alkalinity

B. R. Carter et al.

Title Page

Abstract

Introduction

Conclusions

References

Tables

Figures



Back

Close

Full Screen / Esc

Printer-friendly Version

Interactive Discussion



3 Alk* distributions

The Alk* distribution is affected by both internal and external marine carbonate cycling. Internal cycling is due to net carbonate formation in the surface ocean and net dissolution at depth. External cycling is due to Alk* input by rivers and hydrothermal vent fluids balanced by loss due to burial of biogenic carbonates and authigenic mineralization in sediments. Before showing the global Alk* distribution, we briefly provide background on A_T inputs to the ocean.

The dominant source of Alk* to the ocean is dissolved carbonate minerals in river water, ground water, and hydrothermal vent fluid. For river water with a salinity of 0, Alk* equals the potential alkalinity. This averages around $1100 \mu\text{mol kg}^{-1}$ globally (Cai et al., 2008), but is greater than $3000 \mu\text{mol kg}^{-1}$ for some rivers (Beldowski et al., 2010). Evidence suggests that riverine A_T is increasing due to human activities (Kaushal et al., 2013).

Wolery and Sleep (1988) estimate hydrothermal vents add $0.04 \text{ Pg C yr}^{-1}$ of carbonate to the ocean. This is one fifth of the 0.2 Pg C yr^{-1} riverine source (Cai et al., 2008), though deVilliers (1998) suggested that the hydrothermal contribution may be as high as $0.18 \text{ Pg C yr}^{-1}$.

3.1 Global distribution of Alk*

We map gridded global surface A_T , salinity, Alk*, and phosphate distributions in Fig. 2. Figure 3 shows the surface (top 50 m) distribution of Alk* at the measurement stations. The similarity of the A_T and salinity distributions demonstrates the strong influence of freshwater cycling on the surface marine A_T distribution. The similarity between phosphate and Alk* distributions suggests that Alk* captures the portion of A_T that varies in response to biological cycling as the hard parts of marine organisms. This similarity extends to depth as well. Figures 4 and 5 show zonally-averaged depth sections of Alk* and phosphate from the gridded fields, respectively. The subtropical gyres have the lowest open ocean Alk* in Figs. 2, 3, and 4. Alk* concentrations are high in Arctic

BGD

11, 11139–11178, 2014

Processes
determining marine
alkalinity

B. R. Carter et al.

Title Page

Abstract

Introduction

Conclusions

References

Tables

Figures

◀

▶

◀

▶

Back

Close

Full Screen / Esc

Printer-friendly Version

Interactive Discussion



surface, deep North Indian, and deep North Pacific Oceans. The Alk^* distribution has a broadly similar explanation to the phosphate distribution. A_T uptake to form calcium carbonate reduces surface Alk^* . Dissolution of these carbonates at depth increases Alk^* . The “oldest” water therefore has the highest net Alk^* accumulation. High surface Alk^* in the Southern Ocean and North Pacific is due to upwelled old deep waters.

Several qualitative differences between Alk^* and phosphate are visible in Figs. 2, 4, and 5. Surface phosphate is low in the Bay of Bengal and high in the Arabian Sea, while the opposite is true for Alk^* . Alk^* reaches its highest surface concentration in the Arctic where phosphate is not greatly elevated. These surface differences are due to regional river water Alk^* inputs (Sect. 3.3). Alk^* reaches a maxima below 2000 m in all ocean basins except the Arctic, while phosphate maxima are above 2000 m. We attribute the deeper Alk^* maxima to deeper dissolution of carbonate minerals than organic matter remineralization. Another exception is the higher Alk^* values in the deep Indian Ocean than in the deep Pacific. This is likely due to elevated biogenic carbonate export along the coast of Africa and in the Arabian Sea found by Sarmiento et al. (2002) and Honjo et al. (2008).

3.2 Alk^* by ocean basin

In Fig. 6 we provide 2-D color histograms of surface Alk^* and A_T vs. salinity for the five major ocean basins and indicate the mean A_T and Alk^* for discrete measurement data from each basin. We attribute the decrease in Alk^* as salinity increases – especially visible in lower salinity values in the Arctic Ocean – to mixing between high- Alk^* low-salinity river water and comparatively low- Alk^* high-salinity open ocean water. Precipitation and evaporation in the subtropical gyres widens the histograms across a wide range of salinities and alkalinities without affecting Alk^* . The Alk^* elevation associated with upwelled water is most visible in Fig. 6j where Upper Circumpolar Deep Water upwelling near the Polar Front produces a clump of high Alk^* data lacking the very low-salinity tail characteristic of riverine input. The high Alk^* measurements in Fig. 6d with

BGD

11, 11139–11178, 2014

Processes determining marine alkalinity

B. R. Carter et al.

Title Page

Abstract

Introduction

Conclusions

References

Tables

Figures

⏪

⏩

◀

▶

Back

Close

Full Screen / Esc

Printer-friendly Version

Interactive Discussion



salinity between 32.5 and 33.5 are from the North Pacific Subpolar Gyre, and are also due to upwelled old high- Alk^* water (cf. the Si^* tracer in Sarmiento et al., 2004).

The surface Southern Ocean has the highest Alk^* followed by the Arctic, Pacific, Indian, and Atlantic. The high mean Southern Ocean Alk^* is due to upwelling. The high Arctic surface Alk^* is due to riverine input. The Atlantic and the Arctic together receive ~ 65 % of all river water (Dai and Trenberth, 2002). We construct a riverine A_T budget for the various ocean basins using the following assumptions:

1. the A_T of 25 large rivers are as given by Cai et al. (2008),
2. the volume discharge rates of 200 large rivers are as given by Dai and Trenberth (2002),
3. groundwater and runoff enter each ocean in the same proportion as river water from these 200 rivers,
4. the A_T of all water types that we do not know from assumption 1. is the global mean value estimated by Cai et al. (2008), and
5. 40° N is the boundary between the Atlantic and the Arctic and 40° S is the boundary between the Southern and the Atlantic Oceans (based upon the region of elevated surface phosphate in Fig. 2d),

Our detailed budget is provided as Supplement file SD. We estimate 40 % of continentally derived A_T enters the Atlantic, 20 % enters the Arctic, and 40 % enters all remaining ocean basins. These ocean areas represent 17 %, 5 %, and 78 % of the total surface ocean area in our gridded dataset respectively, so the Arctic receives approximately twice as much riverine A_T per unit area as the Atlantic, and 8 times the rest of the world ocean. The Atlantic has the lowest measured open-ocean surface Alk^* and the lowest basin mean surface Alk^* despite the large riverine sources. The large riverine A_T input must therefore be more than balanced by net calcium carbonate formation. The Indian Ocean also has a low mean surface Alk^* that we attribute to strong

BGD

11, 11139–11178, 2014

Processes determining marine alkalinity

B. R. Carter et al.

Title Page

Abstract

Introduction

Conclusions

References

Tables

Figures



Back

Close

Full Screen / Esc

Printer-friendly Version

Interactive Discussion



net carbonate precipitation. The nearly-zero mean surface Pacific Alk^* indicates that Alk^* supply from upwelling and a small riverine source very nearly balances carbonate precipitation.

3.3 Riverine Alk^* regionally

River water has a high average Alk^* ($1100 \mu\text{mol kg}^{-1}$), so carbonate-rich river discharge can be seen as regionally elevated Alk^* . The total riverine A_T per unit drainage area varies with the quantity of carbonate minerals found in the drainage region (Cai et al., 2008). The A_T load is diluted by total discharge, so high-discharge rivers (e.g. the Amazon and the Congo) often have low Alk^* .

The Amazon River is the largest single riverine marine A_T source. This river has low A_T ($369 \mu\text{mol kg}^{-1}$, Cai et al., 2008), but has the largest water discharge volume of any river, exceeding the second largest – the Congo – by a factor of ~ 5 (Dai and Trenberth, 2002). Consequently, the Amazon discharges approximately 50 % more A_T per year than the river with the second largest A_T discharge, the Changjiang (Cai et al., 2008). The Amazon's influence can be seen as a region of abnormally low salinity and A_T in Fig. 2a and b. Despite the high discharge volume, the influence is only barely visible as a region of elevated Alk^* in Fig. 2c due to the comparatively low Amazon Alk^* . The Amazon's influence is perhaps most easily seen in the elevated Alk^* values in the lowest-salinity data in Fig. 6b. Figure 7 provides a map of Alk^* for this region scaled to show the influence of this low Alk^* river in the Northern Hemisphere (a) winter and (b) summer months. The higher Alk^* found for May through July is consistent with Moore et al. (1986)'s radium isotope based finding that 20–34 % of the surface waters in this region are derived from Amazon during July vs. 5–9 % during December. However, if we assume the Atlantic seawater mixing with the Amazon outflow had an Alk^* of ~ -15 to $0 \mu\text{mol kg}^{-1}$ in December and 45 to $100 \mu\text{mol kg}^{-1}$ in July. We see lower Alk^* values in our distribution and a smaller disparity between winter and summer Alk^* , suggesting a smaller average Amazon influence for the ocean's surface during both seasons than

Title Page

Abstract

Introduction

Conclusions

References

Tables

Figures



Back

Close

Full Screen / Esc

Printer-friendly Version

Interactive Discussion



found by Moore et al. (1986). However, our estimate does not account for any changes in calcium carbonate export induced by nutrient-rich Amazon outflow.

The most visible riverine Alk^* signals are in the Arctic due to the large riverine runoff into this comparatively small basin, the intermediate to high A_T of high latitude river water (Cai et al., 2008), and the confinement of this low-density riverine water to the surface (Jones et al., 2008; Yamamoto-Kawai et al., 2008; Azetsu-Scott et al., 2010). Figure 4d shows the high Arctic Alk^* plume is confined to the top ~ 200 m. Figure 3 shows that these high Alk^* values extend along the coast of Greenland and through the Labrador Sea. Alk^* decreases with increasing salinity in this region (Fig. 6d) due to mixing between the fresh high Alk^* surface Arctic waters and the salty lower Alk^* waters of the surface Atlantic. Gascard et al. (2004a, b) suggest that high Alk^* waters along the coast of Norway are part of the Norwegian Coastal Current, and originate in the Baltic and North Seas where there are also strong riverine inputs (Thomas et al., 2005).

Several mid-latitude rivers empty into marginal seas where PACIFICA, GLODAP, and CARINA have no measurements, so we rely on data published in regional studies. Beldowski et al. (2010) survey the carbonate system in the Baltic Sea and find distributions indicative of mixing with outflow from several rivers. One of these, the Daugava, flows across a limestone rich catchment and has an exceptionally high A_T of $3172 \mu\text{mol kg}^{-1}$. The Mississippi River also has a very high A_T ($2074 \mu\text{mol kg}^{-1}$) (Cai et al., 2008). Keul et al. (2010) report A_T and salinity distributions in waters offshore of the river mouth from which we calculate seawater Alk^* values $> 150 \mu\text{mol kg}^{-1}$. We extrapolate a linear fit of Alk^* against salinity for data collected near the river mouth to 0 salinity to estimate the Mississippi endmember outflow Alk^* as $2201 \mu\text{mol kg}^{-1}$. The Changjiang (Yangtze) River also has an alkaline outflow estimated as $1780 \mu\text{mol kg}^{-1}$ by Cai et al. (2008) and $2874\text{--}3665 \mu\text{mol kg}^{-1}$ by Chen et al. (2005). This river empties into the Yellow Sea where Chou et al. (2009) reported data that we use to estimate an Alk^* of $1978 \mu\text{mol kg}^{-1}$ for the riverine end-member (we assume nitrate concentrations of $5 \mu\text{mol kg}^{-1}$).

**Processes
determining marine
alkalinity**B. R. Carter et al.

[Title Page](#)[Abstract](#)[Introduction](#)[Conclusions](#)[References](#)[Tables](#)[Figures](#)[Back](#)[Close](#)[Full Screen / Esc](#)[Printer-friendly Version](#)[Interactive Discussion](#)

Elevated Alk^* can be seen in the Bay of Bengal with surface values $\sim 100 \mu\text{mol kg}^{-1}$ higher than those in the central Indian Ocean. This bay has two high A_T rivers that join and flow into it, the Brahmaputra ($1114 \mu\text{mol kg}^{-1}$) and the Ganges ($1966 \mu\text{mol kg}^{-1}$) (Cai et al., 2008). Figure 8 provides depth sections for both areas. The riverine Alk^* plume can be clearly seen in the top 50 m of the Bay of Bengal. No similar increase is seen in the Arabian Sea where the Indus River ($1681 \mu\text{mol kg}^{-1}$) discharges only $\sim 1/10$ th of the combined volume of the Brahmaputra and the Ganges.

3.4 Regional inorganic carbonate cycling

The Red Sea portion of Fig. 8 is strongly depleted in Alk^* , and contains the lowest single Alk^* in our dataset, $-247 \mu\text{mol kg}^{-1}$. The Red Sea measurements are from the GEOSECS expedition (Craig and Turekian, 1980), but the very low values are supported by more recent measurements (Silverman et al., 2007). We attribute low Red Sea Alk^* to exceptionally active carbonate mineral formation.

The Red Sea is one of the only regions where carbonate saturation is sufficiently high for inorganic carbonate precipitation to significantly contribute to overall carbonate precipitation (Milliman et al., 1969; Silverman et al., 2007). Notably, saturation remains high at depth in the Red Sea (see Sect. 4.2). Despite this, calcium carbonate sediments in the modern Red Sea are mostly biogenic aragonitic corals and pteropod shells (Gevirtz and Friedman, 1966). However, in this region, pores left as shells dissolve due to sedimentary buildup of carbon dioxide from organic matter remineralization (Hales and Emerson, 1997; Hales, 2003; Boudreau, 2013) are filled in with high-magnesium calcite cement (Almogi-Labin et al., 1986). The hypothesis that inorganic precipitation is an important sink for A_T in the Red Sea is consistent with the prevalence of biogenic calcium carbonate shells if inorganic re-calcification follows sedimentary dissolution of the biogenic carbonates.

Inorganic calcium carbonate has recently been found as metastable ikaite (a hydrated calcium carbonate mineral with the formula $\text{CaCO}_3 \cdot 6\text{H}_2\text{O}$) in natural sea ice

Title Page

Abstract

Introduction

Conclusions

References

Tables

Figures

◀

▶

◀

▶

Back

Close

Full Screen / Esc

Printer-friendly Version

Interactive Discussion



(Dieckmann et al., 2008). Ikaite cycling provides a competing explanation for the high Arctic surface Alk^* values if high A_T low-salinity ikaite-rich ice melt becomes separated from low A_T high-salinity rejected brines. However, riverine A_T inputs are a better explanation: The $\sim 5 \text{ mg ikaite L}^{-1}$ sea ice Dieckmann et al. (2008) found in the Antarctic could only enrich the surface 100 m A_T by $\sim 10 \mu\text{mol kg}^{-1}$ for each meter of ice melted, and Arctic surface Alk^* is elevated by $59 \mu\text{mol kg}^{-1}$ relative to the deeper Arctic in our gridded dataset. By contrast, Jones et al. (2008) estimate a $\sim 5\%$ average riverine end-member contribution to the shallowest 100 m of this region, which accounts for $\sim 55 \mu\text{mol kg}^{-1}$ Alk^* enrichment. Also, surface Alk^* in the Southern Ocean – which has sea ice but lacks major rivers – is not similarly elevated relative to phosphate (Fig. 2) or relative to deep Alk^* (Fig. 4).

4 Controls on the saturation state of calcium carbonate

The Alk^* tracer provides an opportunity to estimate the impact of carbonate cycling on the carbonate mineral saturation, and address the first part of the question we raised in the Introduction. In addition to (1) carbonate cycling, carbonate mineral saturation is affected by (2) organic matter cycling, (3) freshwater cycling, (4) depth changes of seawater, (5) heating and cooling, and (6) A_T changes from nitrogen fixation and denitrification. For each of these six processes, we estimate the standard deviation of the net influence of the process by considering the standard deviation of a “reference” tracer R_i for the process, “ σ_{R_i} ”, where R_i is Alk^* for CaCO_3 cycling, phosphate for organic matter cycling, salinity for freshwater cycling, pressure for depth changes, temperature for heating and cooling, and N^* (Gruber and Sarmiento, 1997) for nitrogen fixation and denitrification. We use the standard deviation of the reference tracer as a measure of the oceanic range of the net influence of the corresponding process. We measure the impact of this range on carbonate mineral saturation using a metric M , which we define

Title Page

Abstract

Introduction

Conclusions

References

Tables

Figures



Back

Close

Full Screen / Esc

Printer-friendly Version

Interactive Discussion



cling (17%), temperature changes (4%), nitrogen fixation and denitrification (1.21%), and freshwater cycling (0.78%).

4.2 Process importance in well-equilibrated surface seawater

We provide M_i values for seawater in the top 50 m of the ocean alongside the R_i , σ_{R_i} , S_{R_i} used to estimate them in Table 2. These surface seawater M_i values are calculated assuming the water remains equilibrated with an atmosphere with 400 μatm $p\text{CO}_2$. We test the validity of this assumption by also estimating M for the observed global $p\text{CO}_2$ variability from incomplete equilibration. However, we do not include this M value estimate in the denominator of Eq. (7) so l values for surface seawater are calculated in the same way as l values from mean seawater globally.

Warming and cooling are the dominant processes controlling Ω_C for well-equilibrated surface seawater (76%). The large increase in M for warming and cooling relative to the value calculated for mean seawater is due to lower equilibrium C_T at higher temperatures. Freshwater cycling is the second most important process (13%), followed by carbonate cycling (8%), organic matter cycling (2%), pressure changes (1%), and denitrification and nitrogen fixation (0.4%). The increased importance of freshwater cycling is because freshwater dilutes C_T by more than the equilibrium C_T decreases from A_T dilution, so carbon uptake tends to follow freshwater precipitation and carbon outgassing follows evaporation. Carbonate cycling is less important because A_T decreases with carbonate precipitation lead to lower C_T at equilibrium. Organic matter cycling is much less important because atmospheric re-equilibration mostly negates the large changes in C_T . Pressure variability is less important simply because we only consider the top 50 m. Our air–sea disequilibrium M estimate suggests surface disequilibria are as important for surface calcite saturation as freshwater cycling, but substantially less important than temperature changes.

The dominance of warming and cooling and freshwater cycling over carbonate cycling is most evident in the Red Sea where high temperatures ($> 25^\circ\text{C}$) and high salinities ($> 40\text{ g kg}^{-1}$) lead to surface calcite saturations exceeding 6 despite extremely low

BGD

11, 11139–11178, 2014

Processes determining marine alkalinity

B. R. Carter et al.

Title Page

Abstract

Introduction

Conclusions

References

Tables

Figures



Back

Close

Full Screen / Esc

Printer-friendly Version

Interactive Discussion



Alk* ($< -200 \mu\text{mol kg}^{-1}$). The deep Red Sea is also warm ($> 20^\circ\text{C}$ at $> 1000\text{ m}$ depth), which keeps $\Omega_{\text{C}} > 3$. The importance of warming and cooling is also evident when considering the broad similarities between the global surface calcite saturation and the surface temperature shown for our gridded dataset in Fig. 9. The lowest surface saturation states correspond to Arctic regions where both the temperature and the salinity are low (see Fig. 2b).

5 Conclusions

Alk* isolates the portion of the A_{T} signal that varies in response to calcium carbonate cycling and the riverine and hydrothermal sources from the portion that varies in response to freshwater and organic matter cycling. The salinity normalization we use has the advantage over previous salinity normalizations that it mixes linearly and changes in a 2 : 1 ratio with C_{T} in response to carbonate cycling. We highlight the following insights from Alk*:

(1) *Alk* distribution*: The Alk* distribution clearly shows the influence of biological cycling including such features as the very low Alk* in the Red Sea due to the high calcium carbonate precipitation there. We also find evidence of strong riverine A_{T} sources near the mouths of several major rivers and in the Arctic. A plot of Alk* against salinity reveals the large A_{T} input from the Amazon River.

(2) *Impact of rivers on carbonate saturation*: Rivers have high Alk* compared to surface waters and might thus be expected to lead to high carbonate ion concentrations. However, because of the low salinity (and hence low A_{T} and calcium ion concentrations), mixing with seawater tends to decrease seawater Ω_{C} . The sensitivities we calculate in Appendix A suggest that a 1 : 1 mixture between river water and surface seawater would have a lower Ω_{C} than surface seawater unless the river water has an Alk* exceeding $\sim 2600 \mu\text{mol kg}^{-1}$. This Alk* is more than twice the $1100 \mu\text{mol kg}^{-1}$ mean riverine A_{T} estimate of Cai et al. (2008). Mixtures of river water and seawater must

BGD

11, 11139–11178, 2014

Processes determining marine alkalinity

B. R. Carter et al.

Title Page

Abstract

Introduction

Conclusions

References

Tables

Figures



Back

Close

Full Screen / Esc

Printer-friendly Version

Interactive Discussion



thus be subjected to net evaporation, net warming, and/or air–sea $p\text{CO}_2$ disequilibrium before Ω_{C} will be in line with typical surface seawater.

(3) *Influence of calcium carbonate cycling on marine calcium carbonate saturation:* Alk^* allows us to quantify the net influence of calcium carbonate cycling on marine calcium carbonate saturation. At the surface, carbonate cycling is less influential for calcite saturation than warming and cooling, air–sea disequilibrium, and freshwater cycling. At depth, the carbonate cycling signal is smaller than the signal from organic matter cycling or pressure changes. In general Alk^* and carbonate saturation are inversely related to each other. For example, subtropical gyres have the highest surface saturation states despite having the lowest open-ocean Alk^* values. Here, high temperatures, strong net evaporation, and lower concentrations of recently-upwelled remineralized C_{T} dominate over the low Alk^* . Similarly, in the deep ocean, saturation is the lowest where A_{T} and thus Alk^* are increasing from calcium carbonate dissolution. This is due to high pressures, low temperatures, and an abundance of remineralized carbon, as discussed by Broecker and Peng (1987). Temperature is the dominant control for surface carbonate saturation globally. This accounts for the low saturation states in the cold surface of the Arctic and Southern Oceans, and high saturations in the warm Red Sea.

The values in Table A3 allow us to compare the impact of the modern anthropogenic atmospheric $p\text{CO}_2$ increase of $\sim 120 \mu\text{atm}$ on CaCO_3 saturation levels to the impact of other climate changes. The increase of $\sim 120 \mu\text{atm}$ is 4.4 times as large as the modern surface ocean $p\text{CO}_2$ standard deviation of $27 \mu\text{atm}$. We calculate this decrease in global surface carbonate ion saturation levels is equivalent to the effect one would get from a ~ 7 to 8°C cooling.

(4) *Monitoring the impact of ocean acidification on carbonate biomineralization with Alk^* :* We propose Alk^* as a model diagnostic that specifically targets calcium carbonate cycling and as a tracer to monitor the impact of ocean acidification on carbonate cycling. Regarding the latter, Ilyina et al. (2009) used models to estimate the biogenic carbonate precipitation response to ocean acidification, and to determine when corresponding A_{T} changes would become detectable by repeat hydrography. However,

BGD

11, 11139–11178, 2014

**Processes
determining marine
alkalinity**

B. R. Carter et al.

Title Page

Abstract

Introduction

Conclusions

References

Tables

Figures



Back

Close

Full Screen / Esc

Printer-friendly Version

Interactive Discussion



A_T varies substantially in response to freshwater cycling that is also changing with climate. Alk^* is mostly insensitive to freshwater cycling, and thus Alk^* trends would better distinguish carbonate cycling shifts from shifts in hydrology.

For related future work, we aim to use the gridded global Alk^* distribution with independent water mixing and transport estimates (Khatiwala et al., 2005, 2007) to infer the magnitude of global sources and sinks of calcium carbonate. We will interpret these estimates in the context of the riverine and hydrothermal sources and sinks of A_T in the ocean, and investigate the degree to which carbonate cycling varies regionally with carbonate saturation.

Appendix A: Definition of the process importance metric M

Our metric for Ω_C variability resulting from the i th process is expressed as M_i :

$$M_i = \sigma_{P_i} \left| \frac{\partial \Omega_C}{\partial P_i} \right| \quad (A1)$$

where P_i is an abstract variable representing the net process influence (that we will later factor out), and $\frac{\partial \Omega_C}{\partial P_i}$ is the calcite saturation sensitivity to the process. We expand $\frac{\partial \Omega_C}{\partial P_i}$ using the chain rule to include a term for Ω_C sensitivity to changes in the reference tracer R_i and a term $\frac{\partial R_i}{\partial P_i}$ representing changes in R_i resulting from the i th process:

$$M_i = \sigma_{P_i} \left| \frac{\partial \Omega_C}{R_i} \frac{\partial R_i}{\partial P_i} \right| \quad (A2)$$

In practice, we calculate Ω_C as a function of $j = 7$ properties: (1) pressure, (2) temperature, (3) salinity, (4) phosphate, (5) silicate, (6) A_T , and (7) C_T for mean seawater and pCO_2 for surface seawater, so we use the chain rule again to further expand the $\frac{\partial \Omega_C}{\partial P_i}$

Title Page

Abstract

Introduction

Conclusions

References

Tables

Figures

◀

▶

◀

▶

Back

Close

Full Screen / Esc

Printer-friendly Version

Interactive Discussion



terms as follows:

$$M_i = \sigma_{P_i} \left| \sum_{j=1}^7 \frac{\partial \Omega_C}{\partial X_j} \frac{\partial X_{j,i}}{\partial R_i} \frac{\partial R_i}{\partial P_i} \right| \quad (\text{A3})$$

Here, the $\frac{\partial X_{j,i}}{\partial R_i}$ are assumed terms (assumptions detailed shortly) that relate the effect of the i th process on the j th property to the effect of the process on R_i , and the $\frac{\partial \Omega_C}{\partial X_j}$ terms reflect calcite saturation sensitivity to changes in the j properties used to calculate it.

We assume the $\frac{\partial X_{j,i}}{\partial R_i}$ terms: we relate changes in temperature from sinking or shoaling to changes in pressure using the potential temperature (θ) routines of Fofonoff and Millard (1983); we assume freshwater cycling linearly concentrates A_T , C_T , phosphate, and silicate by the same ratio that it changes salinity; we relate C_T , phosphate, and A_T changes from organic matter formation to changes in phosphate using the remineralization ratios found by Anderson and Sarmiento (1994) and the empirical relationship of Kanamori and Ikegami (1982); we also use Kanamori and Ikegami (1982)'s constant to relate changes in A_T from nitrogen fixation and denitrification to changes in N^* from these processes; and we assume that an increase in A_T from calcium carbonate dissolution equals the Alk^* increase, and that the corresponding increase in C_T equals half of this Alk^* increase. We neglect any changes in C_T from denitrification and nitrogen fixation because these changes are better thought of as organic matter cycling occurring alongside nitrogen cycling.

We estimate $\frac{\partial \Omega_C}{\partial X_j}$ property sensitivity terms as the differences between Ω_C calculated before and after augmenting j th property by 1 unit. Ω_C is calculated with the MATLAB CO2SYS routines written by van Heuven et al. (2009) using with the carbonate system equilibrium constants of Mehrbach et al. (1973), as refit by Dickson and Millero (1987). Seawater $p\text{CO}_2$ is used in place of C_T for the surface seawater calculations (when $j = 7$) to calculate the change in Ω_C that remains after the surface seawater is allowed to equilibrate with the atmosphere.

Processes
determining marine
alkalinity

B. R. Carter et al.

Title Page

Abstract

Introduction

Conclusions

References

Tables

Figures



Back

Close

Full Screen / Esc

Printer-friendly Version

Interactive Discussion



We assume that the distributions of our R_i reference properties are linearly related to the P_i net activities of their associated processes. This assumption implies:

$$\sigma_P = \sigma_{R_i} \left| \frac{\partial P_i}{\partial R_i} \right| \quad (\text{A4})$$

5 We can then combine Eqs. (A3) and (A4) to obtain:

$$M_i = \sigma_{R_i} \left| \sum_{j=1}^7 \frac{\partial \Omega_C}{\partial X_j} \frac{\partial X_{j,i}}{\partial R_i} \right| = \sigma_{R_i} |S_{R_i}| \quad (\text{A5})$$

10 Here S_{R_i} equals the sum of the terms within the absolute value brackets and represents the calcite saturation sensitivity to a change in the i th process scaled to a unit change in the reference variable for that process. We provide the $\frac{\partial \Omega_C}{\partial X_j}$ and $\frac{\partial X_{j,i}}{\partial R_i}$ values we use to estimate S_{R_i} for atmospherically isolated seawater from all depths in Table A1 and for well-equilibrated surface seawater in Table A2.

15 We use a Monte Carlo analysis to estimate variability and uncertainty in our metric M and our percent relative process importance I calculations. We calculate the standard deviations, σ_M and σ_I , of pools of 1000 M and I estimates calculated after adjusting the seawater properties X_i with a normally-distributed perturbation with a standard deviation equal to the property standard deviation from the gridded dataset. We find $\frac{\sigma_I}{I}$ is typically much smaller than $\frac{\sigma_M}{M}$. This is because carbonate saturation sensitivity is typically proportional to the carbonate saturation itself, so individual Monte Carlo M estimates vary with the initial carbonate saturation and one another. Our σ_M estimates are therefore better thought of as measures of the ranges of sensitivities found in the modern ocean, while σ_I represent variability in the relative importance of processes. We provide σ_M and σ_I for atmospherically isolated seawater globally in Table A3, and for well-equilibrated surface seawater in Table A4.

**Processes
determining marine
alkalinity**

B. R. Carter et al.

Title Page

Abstract

Introduction

Conclusions

References

Tables

Figures



Back

Close

Full Screen / Esc

Printer-friendly Version

Interactive Discussion



Acknowledgements. We thank Eun Young Kwon for contributions to early versions of this research. We also thank the US National Science Foundation for research support (ANT-1040957), as well as the numerous scientists and crew that contributed to the datasets used in this study. R. Key was supported by CICS grant NA08OAR432052.

References

- Almogi-Labin, A., Luz, B., and Duplessy, J.: Quaternary paleo-oceanography, pteropod preservation and stable-isotope record of the Red Sea, *Palaeogeogr. Palaeoclimatol.*, 57, 195–211, doi:10.1016/0031-0182(86)90013-1, 1986.
- Anderson, L. A. and Sarmiento, J. L.: Redfield ratios of remineralization determined by nutrient data analysis, *Global Biogeochem. Cy.*, 8, 65–80, doi:10.1029/93GB03318, 1994.
- Azetsu-Scott, K., Clarke, A., Falkner, K., Hamilton, J., Jones, E. P., Lee, C., Petrie, B., Prinsenberg, S., Starr, M., and Yeats, P.: Calcium carbonate saturation states in the waters of the Canadian Arctic Archipelago and the Labrador Sea, *J. Geophys. Res.-Oceans*, 115, C11, doi:10.1029/2009JC005917, 2010.
- Beldowski, J., Löffler, A., Schneider, B., and Joensuu, L.: Distribution and biogeochemical control of total CO₂ and total alkalinity in the Baltic Sea, *J. Marine Syst.*, 81, 252–259, 2010.
- Boudreau, B. P.: Carbonate dissolution rates at the deep ocean floor, *Geophys. Res. Lett.*, 40, 1–5, doi:10.1029/2012GL054231, 2013.
- Broecker, W. S. and Peng, T. H.: The role of CaCO₃ compensation in the glacial to interglacial atmospheric CO₂ change, *Global Biogeochem. Cy.*, 1, 15–29, 1987.
- Brewer, P. G. and Goldman, J. C.: Alkalinity changes generated by phytoplankton growth, *Limnol. Oceanogr.*, 21, 108–117, 1976.
- Cai, W.-J., Guo, X., Chen, C. A., Dai, M., Zhang, L., Zhai, W., Lohrenz, S. E., Yin, K., Harrison, P. J., and Wang, Y.: A comparative overview of weathering intensity and HCO₃⁻ flux in the world's major rivers with emphasis on the Changjiang, Huanghe, Zhujiang (Pearl) and Mississippi Rivers, *Cont. Shelf Res.*, 28, 1538–1549, 2008.

Processes
determining marine
alkalinity

B. R. Carter et al.

Title Page

Abstract

Introduction

Conclusions

References

Tables

Figures



Back

Close

Full Screen / Esc

Printer-friendly Version

Interactive Discussion



Processes determining marine alkalinity

B. R. Carter et al.

Title Page

Abstract

Introduction

Conclusions

References

Tables

Figures



Back

Close

Full Screen / Esc

Printer-friendly Version

Interactive Discussion



- Chen, J., Wang, F., Meybeck, M., He, D., Xia, X., and Zhang, L.: Spatial and temporal analysis of water chemistry records (1958–2000) in the Huanghe (Yellow River) basin, *Global Biogeochem. Cy.*, 19, GB3016, doi:10.1029/2004GB002325, 2005.
- Chou, W., Gong, G., Sheu, D. D., Hung, C., and Tseng, T.: Surface distribution of carbon chemistry parameters in the East China Sea in summer 2007, *J. Geophys. Res.*, 114, C07026, doi:10.1029/2008JC005128, 2009.
- Craig, H. and Turekian, K. K.: The GEOSECS program 1976–1979, *Earth Planet. Sc. Lett.*, 49, 263–265, doi:10.1016/j.bbr.2011.03.031, 1980.
- Dai, A. and Trenberth, K. E.: Estimates of freshwater discharge from continents: latitudinal and seasonal variations, *J. Hydrometeorology*, 3, 660–687, 2002.
- de Villiers, S.: Excess dissolved calcium in the ocean: a hydrothermal hypothesis, *Earth Planet. Sc. Lett.*, 164, 624–641, 1998.
- Dickson, A. G.: An exact definition of total alkalinity and a procedure for the estimation of alkalinity and total inorganic carbon from titation data, *Deep-Sea Res. A*, 28, 609–623, doi:10.1016/0198-0149(81)90121-7, 1981.
- Dickson, A. G. and Millero, F. J.: A comparison of the equilibrium constants for the dissociation of carbonic acid in seawater media, *Deep-Sea Res. A*, 34, 1733–1743, 1987.
- Dieckmann, G. S., Nehrke, G., Papadimitriou, S., Göttlicher, J., Steininger, R., Kennedy, H., Wolf-Gladrow, D., and Thomas, D. N.: Calcium carbonate as ikaite crystals in Antarctic sea ice, *Geophys. Res. Lett.*, 35, L08051, doi:10.1029/2008GL033540, 2008.
- Feely, R. A., Sabine, C. L., Lee, K., Millero, F. J., Lamb, M. F., Greeley, D., Bullister, J. L., Key, R. M., Peng, T. H., and Kozyr, A.: In situ calcium carbonate dissolution in the Pacific Ocean, *Global Biogeochem. Cy.*, 16, 1144, doi:10.1029/2002GB001866, 2002.
- Fofonof, N. P. and Millard, R. C.: Algorithms for computation of fundamental properties of seawater, *UNESCO R. M.*, 44, 53, <http://hdl.handle.net/1912/2470>, 1983.
- Gascard, J. C., Raisbeck, G., Sequeira, S., Yiou, F., and Mork, K.: Correction to “The Norwegian Atlantic Current in the Lofoten basin inferred from hydrological and tracer data (I-129) and its interaction with the Norwegian Coastal Current”, *Geophys. Res. Lett.*, 31, doi:10.1029/2004GL020006, 2004.
- Gascard, J. C., Raisbeck, G., Sequeira, S., Yiou, F., and Mork, K.: The Norwegian Atlantic Current in the Lofoten basin inferred from hydrological and tracer data (I-129) and its interaction with the Norwegian Coastal Current, *Geophys. Res. Lett.*, 31, L01308, doi:10.1029/2003GL018303, 2004.

**Processes
determining marine
alkalinity**

B. R. Carter et al.

Title Page

Abstract

Introduction

Conclusions

References

Tables

Figures



Back

Close

Full Screen / Esc

Printer-friendly Version

Interactive Discussion



- Gevirtz, J. L. and Friedman, G. M.: Deep-sea carbonate sediments of the Red Sea and their implications on marine lithification, *J. Sediment. Petrol.*, 36, 143–151, 1966.
- Gruber, N. and Sarmiento, J. L.: Global patterns of marine nitrogen fixation and denitrification, *Global Biogeochem. Cy.*, 11, 235–266, 1997.
- 5 Hales, B.: Respiration, dissolution, and the lysocline, *Paleoceanography*, 18, 1099, doi:10.1029/2003PA000915, 2003.
- Hales, B. and Emerson, S.: Calcite dissolution in sediments of the Ceara Rise: in situ measurements of porewater O₂, pH, and CO₂ (aq), *Geochim. Cosmochim. Ac.*, 61, 501–514, 1997.
- 10 Hernández-Ayon, J., Zirino, A., Dickson, A. G., Camiro-Vargas, T., and Alenzuela, E.V: Estimating the contribution of organic bases from microalgae to the titration alkalinity in coastal seawaters, *Limnol. Oceanogr.-Meth.*, 5, 225–232, 2007.
- Honjo, S., Manganini, S. J., Krishfield, R. A., and Francois, R.: Particulate organic carbon fluxes to the ocean interior and factors controlling the biological pump: a synthesis of global sediment trap programs since 1983, *Prog. Oceanogr.*, 76, 217–285, 2008.
- 15 Ilyina, T. R., Zeebe, E., Maier-Reimer, E., and Heinze, C.: Early detection of ocean acidification effects on marine calcification, *Global Biogeochem. Cy.*, 23, GB1008, doi:10.1029/2008GB003278, 2009.
- Jones, E. P., Anderson, L. G., Jutterström, S., Mintrop, L., and Swift, J. H.: Pacific freshwater, river water and sea ice meltwater across Arctic Ocean basins: results from the 2005 Beringia Expedition, *J. Geophys. Res.-Oceans*, 113, doi:10.1029/2007JC004124, 2008.
- 20 Kanamori, S. and Ikegami, H.: Calcium-alkalinity relationship in the North Pacific, *J. Oceanogr.*, 38, 57–62, 1982.
- Kaushal, S. S., Likens, G. E., Utz, R. M., Pace, M. L., Grese, M., and Yepsen, M.: Increased river alkalization in the Eastern US, *Environ. Sci. Technol.*, 47, 10302–10311, doi:10.1021/es401046s, 2013.
- 25 Keul, N., Morese, J. W., Wanninkhof, R., Gledhill, D. K., and Bianchi, T. S.: Carbonate chemistry dynamics of surface waters in the northern Gulf of Mexico, *Aquat. Geochem.*, 16, 337–351, doi:10.1007/s10498-010-9091-2, 2010.
- 30 Key, R. M., Kozyr, A., Sabine, C. L., Lee, K., Wanninkhof, R., Bullister, J. L., Feely, R. A., Millero, F. J., Mordy, C., and Peng, T. H.: A global ocean carbon climatology: results from Global Data Analysis Project (GLODAP), *Global Biogeochem. Cy.*, 18, GB4031, doi:10.1029/2004GB002247, 2004.

Processes determining marine alkalinity

B. R. Carter et al.

Title Page

Abstract

Introduction

Conclusions

References

Tables

Figures



Back

Close

Full Screen / Esc

Printer-friendly Version

Interactive Discussion



Key, R. M., Tanhua, T., Olsen, A., Hoppema, M., Jutterström, S., Schirnack, C., van Heuven, S., Kozyr, A., Lin, X., Velo, A., Wallace, D. W. R., and Mintrop, L.: The CARINA data synthesis project: introduction and overview, *Earth Syst. Sci. Data*, 2, 105–121, doi:10.5194/essd-2-105-2010, 2010.

5 Khatiwala, S.: A computational framework for simulation of biogeochemical tracers in the ocean, *Global Biogeochem. Cy.*, 21, GB3001, doi:10.1029/2007GB002923, 2007.

Khatiwala, S., Visbeck, M., and Cane, M. A.: Accelerated simulation of passive tracers in ocean circulation models, *Ocean Model.*, 9, 51–69, 2005.

10 Milliman, J. D., Ross, D. A., and Ku, T. L.: Precipitation and lithification of deep-sea carbonates in the Red Sea, *J. Sediment. Res.*, 39, 724–736, 1969.

Moore, W. S., Sarmiento, J. L., and Key, R. M.: Tracing the Amazon component of surface Atlantic water using ^{228}Ra , salinity, and silica, *J. Geophys. Res.*, 91, 2574–2580, 1986.

Robbins, P. E.: Oceanic carbon transport carried by freshwater divergence: are salinity normalizations useful?, *J. Geophys. Res.*, 106, 30939–30946, 2001.

15 Sarmiento, J. L., Dunne, J., Gnanadesikan, A., Key, R. M., Matsumoto, K., and Slater, R.: A new estimate of the CaCO_3 to organic carbon export ratio, *Global Biogeochem. Cy.*, 16, 1107, doi:10.1029/2002GB001919, 2002.

Sarmiento, J. L., Gruber, N., Brzezinski, M. A., and Dunne, J. P.: High-latitude controls of thermocline nutrients and low latitude biological productivity, *Nature*, 427, 56–60, 2004.

20 Silverman, Lazar, J. B., and Erez, J.: Effect of aragonite saturation, temperature, and nutrients on the community calcification rate of a coral reef, *J. Geophys. Res.*, 112, CO05004, doi:10.1029/2006JC003770, 2007.

Suzuki, T., Ishii, M., Aoyama, M., Christian, J. R., Enyo, K., Kawano, T., Key, R. M., Kosugi, N., Kozyr, A., Miller, L. A., Murata, A., Nakano, T., Ono, T., Saino, T., Sasaki, K., Sasano, D., Takatani, Y., Wakita, M., and Sabine, C.: PACIFICA Data Synthesis Project, ORNL/CDIAC-159, NDP-092, Carbon Dioxide Information Analysis Center, Oak Ridge National Laboratory, US Department of Energy, Oak Ridge, TN, doi:10.3334/CDIAC/OTG.PACIFICA_NDP092, 2013.

30 Takahashi, T., Sutherland, S. C., Wanninkhof, R., Sweeney, C., Feely, R. A., Chipman, D. W., Hales, B., Friederich, G., Chavez, F., Sabine, C., Watson, A., Bakker, D. C. E., Schuster, U., Metzl, N., Yoshikawa-Inoue, H., Ishii, M., Midorikawa, T., Nojiri, Y., Körtzinger, A., Steinhoff, T., Hoppema, M., Olafsson, J., Arnarson, T. S., Tilbrook, B., Johannessen, T., Olsen, A., Bellerby, R., Wong, C. S., Delille, B., Bates, N. R., and deBarr, J. W.: Climato-

logical mean and decadal change in surface ocean $p\text{CO}_2$, and net sea–air CO_2 flux over the global oceans, *Deep Sea Res. Pt. II*, 56, 554–577, 2009.

Thomas, H., Bozec, Y., de Baar, H. J. W., Elkalay, K., Frankignoulle, M., Schiettecatte, L.-S., Kattner, G., and Borges, A. V.: The carbon budget of the North Sea, *Biogeosciences*, 2, 87–96, doi:10.5194/bg-2-87-2005, 2005.

van Heuven, S., Pierrot, D., Lewis, E., and Wallace, D.: MATLAB Program Developed for CO_2 System Calculations, ORNL/CDIAC-105b, Carbon Dioxide Information Analysis Center, Oak Ridge National Laboratory, US Department of Energy, Oak Ridge, TN, 2009.

Velo, A., Perez, F. F., Brown, P., Tanhua, T., Schuster, U., and Key, R. M.: CARINA alkalinity data in the Atlantic Ocean, *Earth Syst. Sci. Data*, 1, 45–61, doi:10.5194/essd-1-45-2009, 2009.

Wolery, T. J. and Sleep, N. H.: Interactions of geochemical cycles with the mantle, in: *Chemical Cycles in the Evolution of the Earth*, edited by: Gregor, C. B., Garrels, R. M., Mackenzie, F. T., and Maynard, J. B., Wiley, New York, 77–103, 1988.

Wolf-Gladrow, D. A., Zeebe, R. E., Klaas, C., Körtzinger, A., and Dickson, A. G.: Total alkalinity: the explicit conservative expression and its application to biogeochemical processes, *Marine Chem.*, 106, 287–300, 2007.

**Processes
determining marine
alkalinity**

B. R. Carter et al.

Title Page

Abstract

Introduction

Conclusions

References

Tables

Figures



Back

Close

Full Screen / Esc

Printer-friendly Version

Interactive Discussion



Processes determining marine alkalinity

B. R. Carter et al.

Table 1. Metric estimates M_i , relative process importance percentages I_i , calcite saturation sensitivities S_{R_i} to unit changes in the R_i reference properties, and reference property standard deviations σ_{R_i} for the $i = 6$ processes in atmospherically isolated mean seawater from all ocean depths. We provide details on how these terms are estimated and M_i and I_i uncertainties in Appendix A.

Process	i	R_i	S_{R_i}	σ_{R_i}	M_i	I_i
Carbonate cycling	1	Alk*	0.0043	53.5 $\mu\text{mol kg}^{-1}$	0.23	17 %
Org. matter cycling	2	Phosphate	-0.0069	0.60 $\mu\text{mol kg}^{-1}$	0.66	48 %
Freshwater cycling	3	Salinity	0.032	0.27	0.011	0.78 %
Sinking/shoaling	4	Pressure	-0.00028	1411 db	0.4	28 %
Warming/cooling	5	Temp.	0.014	4.20 °C	0.06	4 %
Denit./nit. fix.	6	N^*	-0.010	1.6 $\mu\text{mol kg}^{-1}$	0.017	1.2 %

Title Page

Abstract

Introduction

Conclusions

References

Tables

Figures

◀

▶

◀

▶

Back

Close

Full Screen / Esc

Printer-friendly Version

Interactive Discussion



Processes determining marine alkalinity

B. R. Carter et al.

Title Page

Abstract

Introduction

Conclusions

References

Tables

Figures

◀

▶

◀

▶

Back

Close

Full Screen / Esc

Printer-friendly Version

Interactive Discussion



Table 2. Metric estimates M_i , relative process importance percentages I_i , calcite saturation sensitivities S_{R_i} to unit changes in the R_i reference properties, and reference property standard deviations σ_{R_i} for the $i = 6$ processes in well-equilibrated surface seawater. We provide details on how these terms are estimated and M_i and I_i uncertainties in Appendix A.

Process	i	R_i	S_{R_i}	σ_{R_i}	M_i	I_i
Carbonate cycling	1	Alk*	0.0034	$36.9 \mu\text{mol kg}^{-1}$	0.13	7.8 %
Org. matter cycling	2	Phosphate	-0.0045	$0.51 \mu\text{mol kg}^{-1}$	0.037	2.3 %
Freshwater cycling	3	Salinity	0.20	0.86	0.22	13.2 %
Sinking/shoaling	4	Pressure	-0.00083	15 db	0.011	0.70 %
Warming/cooling	5	Temp.	0.14	8.8°C	1.2	76 %
Denit./nit. fix.	6	N^*	-0.0043	$1.5 \mu\text{mol kg}^{-1}$	0.006	0.40 %
$p\text{CO}_2$ disequilibria	^b	$p\text{CO}_2$	-0.0086	$27 \mu\text{atm}^{\text{a}}$	0.23	^b

^a standard deviation of the Takahashi et al. (2009) revised global monthly $p\text{CO}_2$ climatology

^b the M value for disequilibria is only calculated to test our assumption of surface seawater air–sea equilibration, and is omitted from calculations of I_i for comparison with Table 1.

Processes
determining marine
alkalinity

B. R. Carter et al.

Table A1. $\frac{\partial \Omega_C}{\partial X_j}$ (bold text) and $\frac{\partial X_{j,i}}{\partial R_i}$ (italic text) terms used in Eq. (A5) for atmospherically isolated mean seawater from all ocean depths. These terms are specific to the $j = 7$ (columns) properties we use to calculate Ω_C and $i = 6$ (rows) processes we consider.

Properties units j	Pressure db 1	Temp °C 2	Salinity 3	Phos. $\mu\text{mol kg}^{-1}$ 4	Silicate $\mu\text{mol kg}^{-1}$ 5	A_T $\mu\text{mol kg}^{-1}$ 6	C_T $\mu\text{mol kg}^{-1}$ 7
Mean seawater values	2235	3.7	34.71	2.15	49.0	2362	2254
Process i	-0.00028	0.014	-0.011	-0.0085	-0.00012	0.0082	-0.0079
Carbonate cycling	1	–	–	–	–	1	0.5
Org. matter cycling	2	–	–	1	–	-20.16	117
Freshwater cycling	3	–	1	0.062	1.4	68	65
Sinking/shoaling	4	1	0.00010	–	–	–	–
Warming/cooling	5	–	1	–	–	–	–
Denit./nit. fix.	6	–	–	–	–	-1.26	–

Title Page

Abstract

Introduction

Conclusions

References

Tables

Figures

◀

▶

◀

▶

Back

Close

Full Screen / Esc

Printer-friendly Version

Interactive Discussion



Processes determining marine alkalinity

B. R. Carter et al.

Table A2. $\frac{\partial \Omega_C}{\partial X_j}$ (bold text) and $\frac{\partial X_{j,i}}{\partial R_i}$ (italic text) terms used in Eq. (A5) for well-equilibrated surface seawater. These terms are specific to the $j = 7$ (columns) properties we use to calculate Ω_C and $i = 6$ (rows) processes we consider.

Properties	Pressure	Temp	Salinity	Phos.	Silicate	A_T	$p\text{CO}_2$	
units	db	°C		$\mu\text{mol kg}^{-1}$	$\mu\text{mol kg}^{-1}$	$\mu\text{mol kg}^{-1}$	μatm	
j	1	2	3	4	5	6	7	
Mean seawater values	25	18.3	34.82	0.51	2.5	2305	350	
Process	i	-0.00084	0.14	-0.022	-0.0038	-0.00013	0.0034	-0.0086
Carbonate cycling	1	–	–	–	–	<i>1</i>	–	
Org. matter cycling	2	–	–	<i>1</i>	–	<i>-20.16</i>	–	
Freshwater cycling	3	–	<i>1</i>	<i>0.015</i>	<i>0.072</i>	<i>65.9</i>	–	
Sinking/shoaling	4	<i>1</i>	<i>0.00010</i>	–	–	–	–	
Warming/cooling	5	–	<i>1</i>	–	–	–	–	
Denit./nit. fix.	6	–	–	–	–	<i>-1.26</i>	–	

Title Page

Abstract

Introduction

Conclusions

References

Tables

Figures

◀

▶

◀

▶

Back

Close

Full Screen / Esc

Printer-friendly Version

Interactive Discussion



Processes determining marine alkalinity

B. R. Carter et al.

[Title Page](#)

[Abstract](#)

[Introduction](#)

[Conclusions](#)

[References](#)

[Tables](#)

[Figures](#)



[Back](#)

[Close](#)

[Full Screen / Esc](#)

[Printer-friendly Version](#)

[Interactive Discussion](#)



Table A3. Monte Carlo derived estimates for M_i variability (σ_{M_i}) and I_i variability (σ_{I_i}) for atmospherically-isolated mean seawater from all ocean depths.

Process	i	σ_{M_i}	σ_{I_i}
Carbonate cycling	1	0.09	1 %
Org. matter cycling	2	0.2	3 %
Freshwater cycling	3	0.006	0.08 %
Sinking/shoaling	4	0.2	5 %
Warming/cooling	5	0.02	2 %
Denit./nit. fix.	6	0.006	0.1 %

Processes determining marine alkalinity

B. R. Carter et al.

Title Page

Abstract

Introduction

Conclusions

References

Tables

Figures



Back

Close

Full Screen / Esc

Printer-friendly Version

Interactive Discussion



Table A4. Monte Carlo derived estimates for M_i variability (σ_{M_i}) and I_i variability (σ_{I_i}) for well-equilibrated surface seawater.

Process	i	σ_{M_i}	σ_{I_i}
Carbonate cycling	1	0.03	0.8%
Org. matter cycling	2	0.01	0.2%
Freshwater cycling	3	0.04	0.5%
Sinking/shoaling	4	0.001	0.03%
Warming/cooling	5	0.2	1%
Denit./nit. fix	6	0.002	0.04%
$p\text{CO}_2$ disequilibria	^a	0.05	^a

^a disequilibria are included only as a test of our assumption of surface seawater air–sea equilibration, so these M_i values are omitted from calculations of I_i .

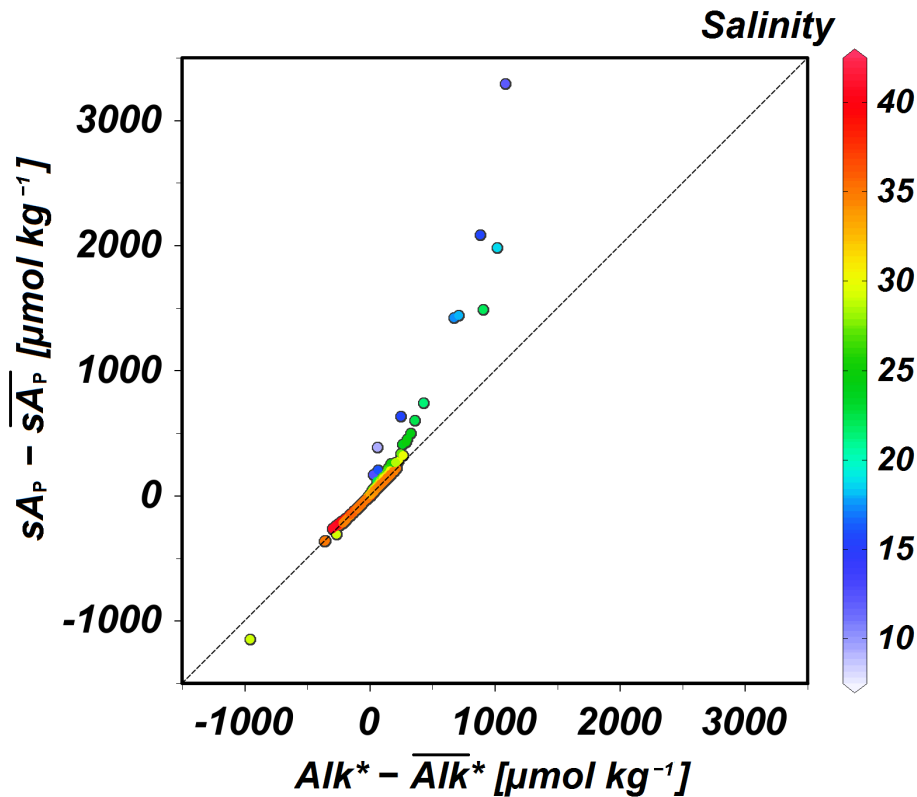


Figure 1. Mean subtracted traditionally normalized potential alkalinity, sA_P , plotted against mean subtracted Alk^* for all data in our merged CARINA, PACIFICA, and GLODAP bottle data product. Salinity is indicated by dot color. The vast majority of data fall near the dashed 1 : 1 line which we provide for reference. However, the large deviations from this line, dominantly in low-salinity Arctic data, demonstrate the non-linearity of the traditional salinity normalization sA_P .

Processes determining marine alkalinity

B. R. Carter et al.

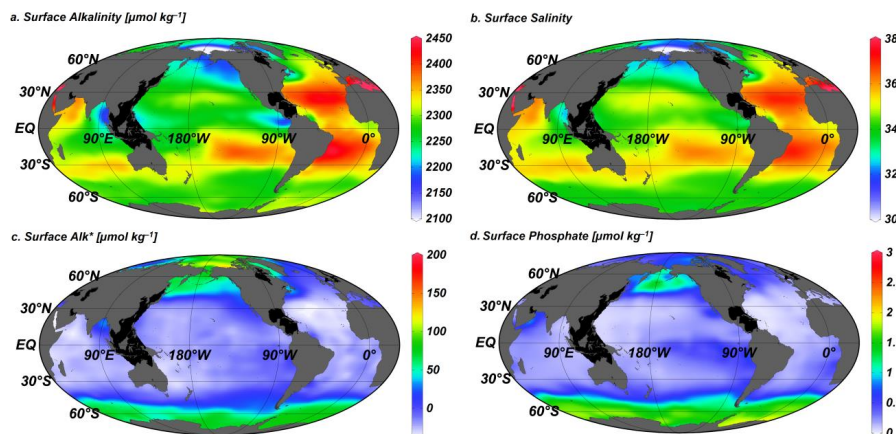


Figure 2. Global (a) total alkalinity A_T , (b) salinity, (c) Alk^* , and (d) phosphate distributions at the surface (10 m depth surface) from our gridded CARINA, PACIFICA, and GLODAP bottle data product. Areas with exceptionally poor coverage in the data used to produce the gridded product are blacked out.

[Title Page](#)[Abstract](#)[Introduction](#)[Conclusions](#)[References](#)[Tables](#)[Figures](#)[Back](#)[Close](#)[Full Screen / Esc](#)[Printer-friendly Version](#)[Interactive Discussion](#)

Processes determining marine alkalinity

B. R. Carter et al.

Title Page

Abstract

Introduction

Conclusions

References

Tables

Figures



Back

Close

Full Screen / Esc

Printer-friendly Version

Interactive Discussion

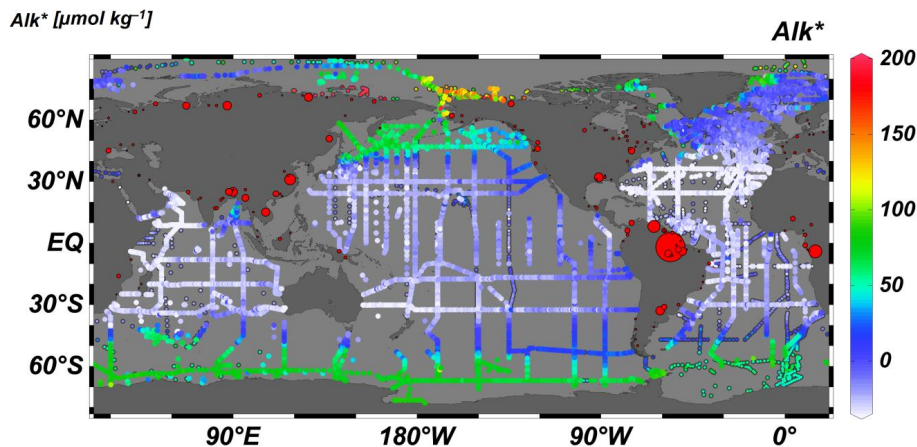


Figure 3. Alk^* values (in $\mu\text{mol kg}^{-1}$) in top 50 m of the ocean plotted in color. Points with black borders indicate that either A_T was measured prior to 1992 (i.e. before reference materials were commonly used) or that no nitrate value was reported (in which case a nitrate concentration of $5 \mu\text{mol kg}^{-1}$ is assumed). Red dots on land indicate the locations and mean annual discharge volumes (indicated by dot size) of 200 large rivers, as given by Dai and Trenberth (2002).

Processes
determining marine
alkalinity

B. R. Carter et al.

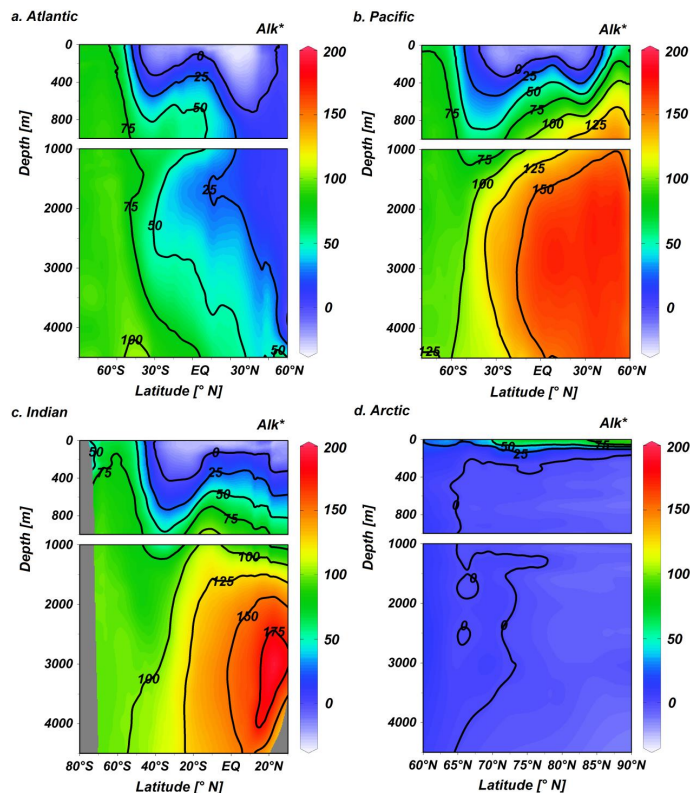


Figure 4. Zonal mean Alk^* distributions (in $\mu\text{mol kg}^{-1}$) in the **(a)** Atlantic, **(b)** Pacific, **(c)** Indian, and **(d)** the Arctic oceans plotted against latitude and depth.

Title Page

Abstract

Introduction

Conclusions

References

Tables

Figures



Back

Close

Full Screen / Esc

Printer-friendly Version

Interactive Discussion



Processes
determining marine
alkalinity

B. R. Carter et al.

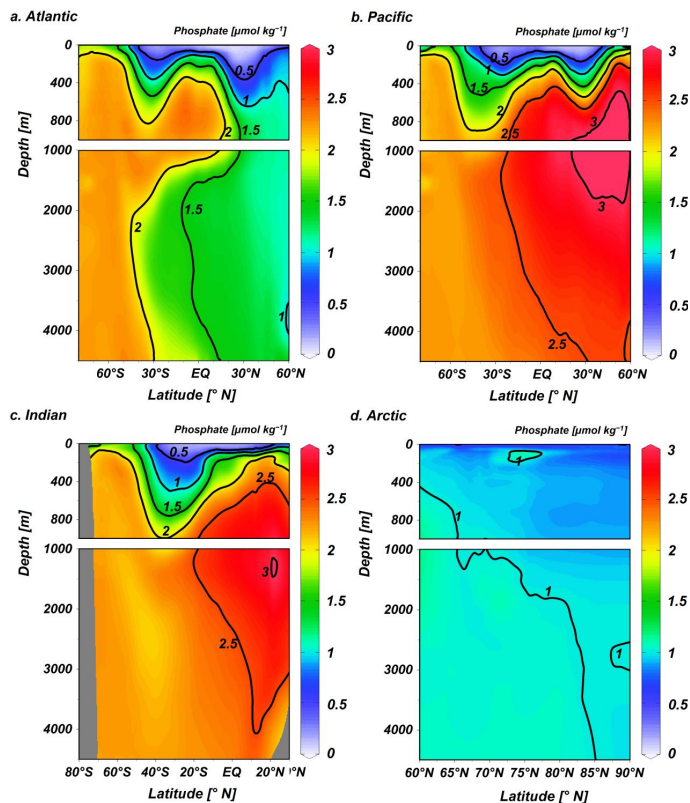


Figure 5. Zonal mean phosphate distributions (in $\mu\text{mol kg}^{-1}$) in the (a) Atlantic, (b) Pacific, (c) Indian, and (d) the Arctic oceans plotted against latitude and depth.

Title Page

Abstract

Introduction

Conclusions

References

Tables

Figures



Back

Close

Full Screen / Esc

Printer-friendly Version

Interactive Discussion



Processes
determining marine
alkalinity

B. R. Carter et al.

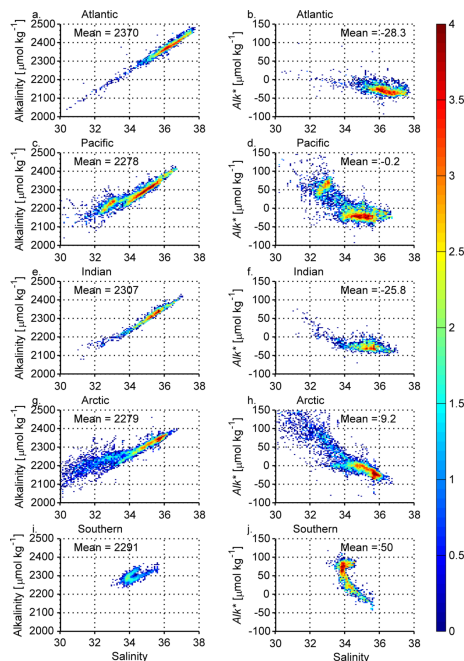


Figure 6. 2-D histograms indicating the log (base 10) of the number of measurements that fall within bins of A_T (**a, c, e, g, i**) and Alk^* (**b, d, f, h, j**) vs. salinity with color. Data are limited to the top 50 m of the (**a, b**) Atlantic, (**c, d**) Pacific, (**e, f**) Indian, (**g, h**) Arctic, and (**i, j**) Southern Oceans. Due to the log scale, the vast majority of the measurements are found in the warmer colored bins. Where basins connect, the boundary between the Atlantic and the Arctic oceans is 40° N, between the Atlantic and the Indian is 20° E, between the Indian and the Pacific is 131° E, between the Pacific and the Atlantic is 70° W, and between the Southern Ocean and the other oceans is 40° S.

Processes determining marine alkalinity

B. R. Carter et al.

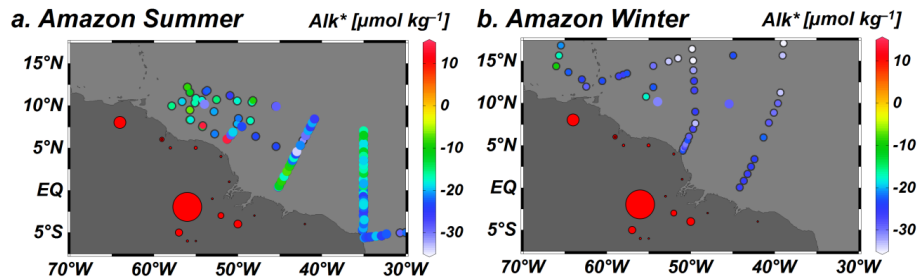


Figure 7. Alk^* (in $\mu\text{mol kg}^{-1}$) in top 50 m of the ocean near the Amazon River outflow plotted in color, though with a narrower color scale than is used for all other plots. Panel (a) is limited to data collected in November through January, and in panel (b) is limited to measurements from May through July. The higher Alk^* values in Northern Hemisphere summer months are consistent with observations of higher quantities of Amazon-derived water during these months (Moore et al., 1986). Points with black borders indicate that either the A_T was measured prior to 1992 (before reference materials were commonly used) or that no nitrate value was reported (in which case a nitrate concentration of $5 \mu\text{mol kg}^{-1}$ is assumed). Red dots on land indicate the locations and mean annual discharge volumes (indicated by dot size) of 200 large rivers, as given by Dai and Trenberth (2002).

Title Page

Abstract

Introduction

Conclusions

References

Tables

Figures

◀

▶

◀

▶

Back

Close

Full Screen / Esc

Printer-friendly Version

Interactive Discussion



Processes
determining marine
alkalinity

B. R. Carter et al.

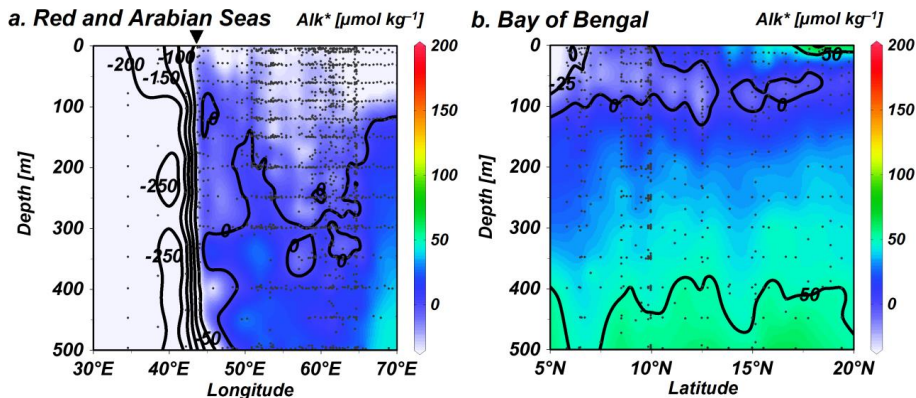


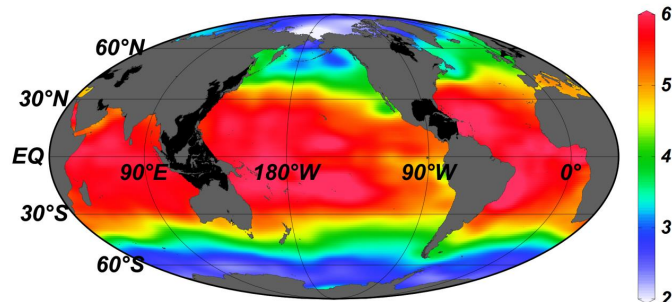
Figure 8. Alk* distributions (in $\mu\text{mol kg}^{-1}$) **(a)** between 5° and 30° N in the Red and Arabian Seas shown against longitude, and **(b)** between 75° and 100° E in the Bay of Bengal plotted against latitude. Small black dots indicate where data is present. The inverted triangle above **(a)** indicates the longitude of the mouth of the Red Sea.

[Title Page](#)[Abstract](#)[Introduction](#)[Conclusions](#)[References](#)[Tables](#)[Figures](#)[◀](#)[▶](#)[◀](#)[▶](#)[Back](#)[Close](#)[Full Screen / Esc](#)[Printer-friendly Version](#)[Interactive Discussion](#)

Processes determining marine alkalinity

B. R. Carter et al.

a. Surface Calcite Saturation



b. Surface Temperature [°C]

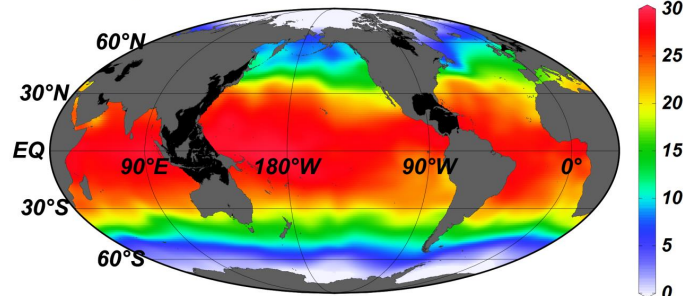


Figure 9. Gridded global (a) calcite saturation, and (b) temperature at the surface (10 m depth surface) of our gridded CARINA, PACIFICA, and GLODAP bottle data product. Areas with exceptionally poor coverage in the data used to produce the gridded product are blacked out.

Title Page

Abstract

Introduction

Conclusions

References

Tables

Figures



Back

Close

Full Screen / Esc

Printer-friendly Version

Interactive Discussion

